Sheffield Hallam University

Impact of thermal processing or solvent casting upon crystallization of PLA nanocellulose and/or nanoclay composites

TRIFOL, J, VAN DRONGELEN, M., CLEGG, Francis <http://orcid.org/0000-0002-9566-5739>, PLACKETT, D., SZABO, P. and DAUGAARD, A.E.

Citation:

Impact of thermal processing or solvent casting upon crystallization of PLA nanocellulose and/or nanoclay composites

J. Trifol[a], M. van Drongelen[a], F.Clegg[b], D. Plackett[c], P. Szabo[a], A. E. Daugaard[a]

[a] *Danish Polymer Centre, Department of Chemical and Biochemical Engineering, Søltofts Plads, Technical University of Denmark, Building 229, DK – 2800, Kgs. Lyngby, Denmark*

[b] *Materials and Engineering Research Institute, Sheffield Hallam University, Howard Street, Sheffield, S1 1WB, U.K.*

[c] *Faculty of Pharmaceutical Sciences, University of British Columbia, 2405 Westbrook Mall, Vancouver, BC V6T 1Z3, Canada*

Abstract:

Here we present how processing (solvent casting or isothermal crystallization) impacts crystallinity of poly(lactic acid) (PLA) and its nanocomposites (PLA/1wt% cellulose nanofibers (CNF), PLA/1wt% nanoclay (C30B) or PLA/1wt% CNF/1wt% C30B. Polarized optical microscopy demonstrated a heterogeneneous nucleation process during isothermal crystallization leading to smaller homogeneously distributed spherulites. With solvent casting, no effect on morphology was observed with respect to the nanoparticles, but an increased spherulite size was observed at higher temperatures. This fact raises significant concerns regarding the suitability of solvent casting as a lab-scale procedure to investigate materials. Additionally, combining the reinforcing agents, CNF and C30B, did not increase nucleation rate, in contrast with the general tendency, where the incorporation of both particles led to improved properties (e.g., thermomechanical and barrier properties). However, a combination of C30B and CNF did lead to an overall increase in the rigid amorphous fraction (RAF) and a reduced mobile amorphous fraction (MAF).

1. INTRODUCTION

The extensive use of non-renewable resources is a well-known and serious global issue. Petroleum reserves are continually being depleted and since most plastics made from these reserves are non-biodegradable, their disposal is a problem. In this context, substituting petroleum-based plastics with bio-based and biodegradable alternatives is an attractive proposition for sustainable development. Nevertheless, bio-based polymers such as poly (lactic acid) (PLA) still suffer from practical drawbacks such as brittleness, poor thermomechanical properties, and slow crystallization leading to longer processing times and modest gas barrier properties [1,2] when compared to currently used petrochemical-derived plastics. Consequently, considerable efforts have been focused towards improving the properties of bio-based polymers in general, and PLA in particular. These include the reinforcement of PLA with different types of nanoparticles such as nanocellulose [3], nanoclay [4], or a combination of both [5,6].

Briefly, PLA is a biodegradable, thermoplastic aliphatic polyester obtained from the ring-opening polymerization of lactide [7], which is produced from the dehydration of lactic acid obtained from different

40 renewable resources. Nanoclays are composed of several layers of inorganic platelets stacked on top of each

41 other, with platelet diameters in the range of 100 to 1000 nm and thickness <1 nm. In this study, commercially

42 available, organically modified clay (Cloisite® 30B abbreviated to C30B) was used. In this clay the platelets are

43 surface modified with hydrophobic bis (2-hydroxy-ethyl)-methyl tallow alkyl ammonium cations [8]. Cellulose

44 nanofibers (CNF) have lengths close to or in the microscale and diameters in the nanoscale. CNF typically

45 exhibit hydroxyl (or carboxylate [9]) groups on the nanofiber surfaces, but the CNF used in this work was partially

46 acetylated during the CNF extraction procedure, presenting a small amount of acetyl groups on the surface

47 (degree of substitution or DS ~ 10%) and slightly decreasing the hydrophilic character of the CNF [10].

48

49 In our previous studies[2], it was found that the incorporation of 1% CNF in solvent-cast PLA led to a reduction of

50 63% in Oxygen Transmission Rate (OTR), whereas with the equivalent composite containing 1% C30B only a

51 26% decrease was observed. Nanoclay has a higher surface-to-volume ratio than CNF, where a fully exfoliated

52 platelet of dimensions 400 x 300 x 1 nm [11] has an approximate surface to volume ratio of 2×10^9 m^{-1}, while fibers

53 of 25 nm diameter and 650 nm length exhibit only a surface to volume ratio of 1.6×10^8 m^{-1}. Platelet-shaped

54 morphologies therefore have 12.5 times higher surface-to-volume ratio, and would therefore be expected to

55 improve the barrier properties more efficiently than the CNF. However, the CNF-based composites were

56 showing better barrier properties than C30B. Considering this factor, it would be reasonable to suggest that part

57 of the improvement in barrier properties for CNF composites, could be due to crystallinity effects originating

58 from the fibers that is not happening on the C30B. Crystallinity is well known to have a positive impact on

59 properties of materials such as gas barrier [12,13] or mechanical properties [14–18]. The crystallization properties of

60 PLA [14,19,20] and PLA-based nanocomposites, such as PLA/CNF [18], PLA/C30B [13], and even PLA/based

61 composites with banana fibers and clay [21] have been the subject of earlier studies. Differential scanning

62 calorimetry (DSC) has revealed that both CNF- and C30B-containing PLA composites show a similar degree of

63 crystallinity, while still exhibiting significantly different barrier properties. Therefore, this study was conducted

64 to investigate the differences in crystallinity and morphology induced by the different types of reinforcing

65 agents.

66

67 Crystallinity is a broad topic that, especially in composite literature, has typically been described using only the

68 degree of crystallinity, albeit other crystallinity-related parameters, such as polymorphism and the rigid

69 amorphous fraction (RAF) could affect polymer properties. Crystalline PLA exhibits multiple polymorphic

70 phases, namely α , β and γ, (and η stereocomplex [22]) and it has been found that the prevailing α form exists as

71 two different polymorphs (α = ordered and α´ = disordered) which have different chain packing [23]. In addition,

72 it has been widely accepted that the amorphous region of semi-crystalline polymers is itself composed of two

73 fractions—the mobile amorphous fraction (MAF), which shows chain mobility, and the rigid amorphous

74 fraction (RAF), an intermediate confined nanophase [24]. Classically, it has been considered that the RAF is

75 present at the interface between the crystals and the surrounding amorphous phase; however, nanoparticles can

76 also induce a confined nanophase wherein conformational rearrangements may occur, the so-called "cooperative

77 rearrangement region" (CRR) [25], for this reason some authors distinguish the RAF generated by crystallinity

78 (RAF_{CRYST}) from the RAF created by nanoparticles (RAF_{NANO}). Despite the complexity of crystallinity,

79 understanding the critical parameters that affect materials properties can prove helpful towards achieving an

80   optimal material performance.

81

82   One of the major potential applications of bio-based polymers is in bio-based packaging materials. There are

83   three critical parameters for such applications to be realized that can be affected by the crystallinity of the

84   materials. The first parameter, mass transport/barrier properties, controls the quality of the contained food and

85   the impact of crystalline morphology on water vapor transport is currently under investigation[26]. The second

86   parameter, transparency, is evaluated in the present work and is highly relevant in films for food packaging

87   applications [27] since customers may want to clearly see the food before purchasing. Generally, an increased

88   crystallinity can improve certain properties, but it can also decrease optical transparency [2] as a result of

89   scattering of light due to the different densities between crystalline and amorphous domains. The third

90   parameter, thermal transitions (i.e. T_g and T_m), is also evaluated herein and can be influenced by crystallinity,

91   which significantly affects material processing.

92

93   Here we investigate the differences in crystallinity induced by nanocellulose and nanoclay as well as the

94   influence of combining both types of particles, while providing an insight into differences in crystallinity

95   induced by solvent casting and isothermal crystallization. Solvent casting is widely used to investigate the

96   impact of nanoparticles on polymer properties. However, traditionally, except for some recent techniques such

97   as electrospinning [28], or the use of 3D printed sacrificial molds [29], industrially relevant techniques usually relies

98   on higher processing temperatures. Depending on processing and crystallization behavior, different

99   nanoparticles can have a different impact on crystallization, and solvent casting might therefore not accurately

100   predict the performance of nanocomposites processed in more conventional processes at high temperature.

101

102   **2.   EXPERIMENTAL**

103

104   **2.1 Materials and methods**

105   L-PLA (Ingeo 2003D) was supplied by Natureworks (Minnesota, USA). The clay used for this study was

106   Cloisite® C30B and was supplied by Southern Clay Products (Texas, USA). C30B is a commercially available

107   clay comprehensively described in the literature [30–32]. The extraction of nanocellulose CNF [10] and the

108   preparation of nanocomposites have been described in more detail elsewhere [2,5] though a short summary is

109   presented below.

110

111   **2.2 Nanocomposite preparation**

112   2.2.1 CNF extraction [10]

113   The CNF extraction procedure as well as its characterization has been already pusblished[10]. Briefly, 50 g of sisal

114   fibers were cleaned overnight with 1.5 L of aqueous NaOH solution (2 wt%) at room temperature, and after

115   filtration the fibers were alkali-treated three times with 1.5 L of aqueous NaOH solution (10 wt%) at boiling

116   point over 1.5 h. The mercerized fibers were bleached with 1.25 mL of water at 70°C, 8 mL of acetic acid and

117   40 mL of $NaClO_2$ added every hour for 7 hours. Subsequently, the fibers were acetylated using 900 mL of a

118   solution of HNO_3/acetic acid (1:6 v/v) at boiling point for 90 minutes. After that, the pulp was solvent

119   exchanged in dimethylformamide (DMF). A 1 wt% solution of acetylated pulp in DMF was then dispersed for

120   72 hours with vigorous magnetic stirring followed by centrifugation at 2500 rpm for 10 mins to remove any

121   remaining aggregates, the supernatant was used to prepare the nanocomposites.

122

123

124   2.2.2 Nanocomposite preparation via solvent casting

125   Briefly, PLA and nanoparticles were dissolved/dispersed separately in a solvent, and subsequently the solution

126   of PLA and the suspension of nanoparticles were mixed and cast in a Teflon mold, and the solvent was removed

127   by evaporation. Due to the different nature of the particles, an optimized protocol was used for each

128   combination.

129

130   2.2.2.1 PLA and PLA/C30B nanocomposites

131   Neat PLA and PLA/C30B (1wt% of clay) nanocomposites were prepared using dichloromethane (DCM) as a

132   solvent. In total, 10 g of PLA was dissolved in 200 mL of DCM, and the mixture was kept under magnetic

133   stirring in a sealed flask overnight. Separately, 3 g of C30B was mixed with 300 mL of DCM and kept under

134   magnetic stirring for 24 hours. Subsequently, the clay suspension was ultrasonicated for 3 hours at 200W and

135   then homogenized for 90 minutes with an Ultra-Turrax homogenizer (Jonke & Kunnel IKA Ultra-Turrax T25)

136   at 20500 rpm. The PLA solution and nanoclay suspension were mixed to obtain the desired concentration of

137   C30B in PLA and a final volume of 250 mL obtained by dilution with DCM. Thereafter the mixture was

138   magnetically stirred, ultrasonicated for 90 minutes, homogenized for 30 minutes and finally degassed by

139   ultrasonication for 5 minutes. Next, 80 mL of the suspension was poured slowly into a Teflon mold covered by a

140   5-13 μm filter paper into a Climacell climatic chamber, which was kept at 23ºC for 16 h. Finally, the films were

141   removed from the Teflon mold and further dried at 50ºC under vacuum for at least 24 hours to remove the

142   remaining traces of DCM.

143

144   2.2.2.2 PLA/CNF and PLA/CNF/C30B nanocomposites

145   The PLA/CNF and PLA/CNF/C30B nanocomposites (1wt% of each nanoparticle) were prepared using

146   dimethylformamide (DMF) as a solvent. A total of 3.3 g of PLA was dissolved in 66 mL of DMF, whilst kept

147   for 2 h at 70ºC under vigorous magnetic stirring. Separately, 2 g of C30B was mixed with 200 mL of DMF and

148   the mixture was kept under strong magnetic stirring for 24 h at room temperature. Next, the nanoclay suspension

149   was ultrasonicated for 3 hours at 200W and thereafter homogenized for 90 min at 20500 rpm using an Ultra-

150   Turrax homogenizer. Finally, the required amounts of the PLA, CNF, and C30B solutions or suspensions were

151   mixed by magnetic stirring and poured slowly into a Teflon mold, where they were dried for 15 h at 80°C and

152   subsequently for 24 h at 50°C under vacuum.

153

154   2.2.2.3 Thermal treatments

155   Solvent-cast materials were treated to obtain amorphous and isothermally crystallized products. In order to

156   obtain fully amorphous specimens for UV-Vis spectroscopy and room temperature X-ray diffraction (XRD)

157   measurements, solvent-cast products were placed between two aluminum foils and then subsequently hot

158   pressed for 5 mins at 170°C, followed by fast cooling with water (at 10°C) (quenching). Thereafter, the fully

amorphous materials were isothermally crystallized for two hours at the corresponding crystallization temperature in an oven to achieve crystallized materials.

For other measurements including dynamic differential scanning calorimetry (DSC), temperature-modulated differential scanning calorimetry (MDSC), polarized optical microscopy (POM) and X-ray diffraction (XRD), the formation of fully amorphous materials and their isothermal crystallization at specified temperatures was performed in the instruments themselves as described in the corresponding sections.

2.3 Characterization

2.3.1 Polarized Optical Microscopy

Isothermal crystallization of the PLA and its nanocomposites was evaluated by polarized optical microscopy (POM) using a Nikon Eclipse E100 microscope with a Mettler Toledo FP82HT hot-stage at 140°C, 120°C, and 100°C. Fully amorphous samples were obtained from solvent-cast materials by inserting them between two microscope slides and placing them on the microscope hot stage, which was preheated to 200°C. After 2 minutes the samples were removed and cooled as quickly as possible with a tissue impregnated with ethanol. The sample was replaced on the hot stage after it reached the desired isothermal crystallization temperature and photographs were taken at regular intervals.

2.3.2 DSC

Isothermal crystallization kinetics were evaluated using a TA Instruments DSC Q1000 and the protocol illustrated in Figure 1. First, any crystallinity in the solvent cast materials dictated by the thermal history of the nanocomposites was erased by heating the samples at 10°C/min up to 200°C (1), maintaining the sample for two mins at 200°C (2), and then cooling at 20°C/min to 0°C (3). Thereafter, the samples were raised to the desired isothermal crystallization temperature (140°C, 120°C, 100°C or 80°C) at 10°C/min (4), and kept for 2 hours at that temperature (5). Finally, the samples were cooled to 0°C at 20°C/min (6) and then heated to 200°C at 10°C/min (7). The glass transition, T_g, and melting temperature, T_m (from the maximum of the melting peak), were determined during this final heating run. No crystallization peaks were observed during any of the cooling cycles indicating that no significant crystallization occurred during this part of the treatment.
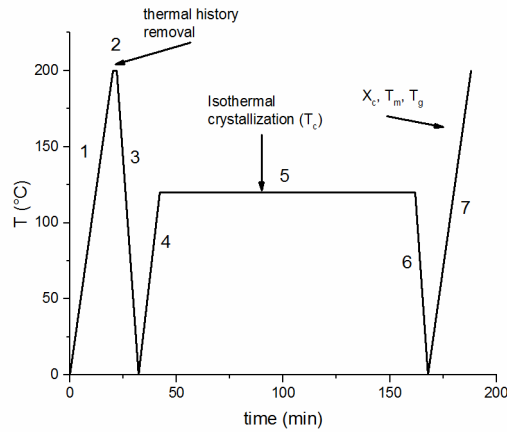
The areas under the crystallization peaks obtained during the isothermal crystallization cycles (5) were integrated using TA Instruments Universal Analysis Software. The baseline was extrapolated from the heat flow signal after crystallization of the material was complete. The resulting area was integrated and the half crystallization time was considered as the time when 50% of maximum crystallinity was reached.

The heat capacity variation (ΔCp) values of PLA and its nanocomposites when in a fully amorphous state at their corresponding T_g was determined in triplicate using a TA Instruments Discovery DSC. The samples were submitted to a thermal treatment similar to stages (1-4) described in Figure 1, but cycle 4 heating was done until 200°C. This was made to erase all of the thermal story of the samples and therefore measure the heat capacity variation (ΔCp) when fully amorphous.

2.3.3   MDSC

The advantage of utilizing MDSC over DSC is that heat flow due to crystallization (termed reversible enthalpy) can be separated from that due to melting (termed non-reversible enthalpy), enabling a more accurate determination of the degree of crystallinity. MDSC was performed using a TA Instruments DSC Q1000 and a cycle similar to the protocol described in Figure 1, albeit with a modulation cycle (Amplitude = ±0.50°C, period = 30 s) during the final heating stage (stage 7).

To determine the degree of crystallinity (X_c), Eq 1 was used:

$$Xc = \frac{\Delta H_{nonrev} - \Delta H_{rev}}{\Delta H_0} \quad (Eq\ 1)$$

where X_c is the degree of crystallinity of the composite, ΔH_{nonrev} is the non-reversible enthalpy, and ΔH_{rev} is the reversible enthalpy. A melting enthalpy, ΔH_0, of 106 J g^{-1} for 100% crystalline α−poly (L-lactide) was used as reported [33], while an enthalpy 25 J g^{-1} lower (81 J g^{-1}) was considered for the α' phase, as suggested in the literature [34]. Again, no crystallization peaks were observed during the cooling cycles.

The mobile amorphous fraction (MAF) and rigid amorphous fraction (RAF) in the nanocomposites were determined by adapting an existing protocol for PLA [35]. Instead of only comparing the heat capacity of a specimen to the heat capacity of neat amorphous PLA (therefore different specimens), accuracy was improved by using the fully amorphous specimen (PLA or its nanocomposites) as reference to evaluate the relative impact of each crystalline morphology in the same treated material. Thereafter, these values were normalized using the heat capacity of PLA and nanocomposites. The reason for this was that PLA and its nanocomposites when in their fully amorphous phase showed different heat capacities due to the presence of nanoparticles affecting the amount of RAF.

The MAF was therefore determined by means of Eq 2.

$$\% \, MAF = \frac{\Delta Cp \, \Delta Cp_{MAT}}{\Delta Cp' \, \Delta Cp_{PLA}} * 100 \, (Eq \, 2)$$

where ΔCp_{PLA} is the heat capacity variation of fully amorphous PLA, while ΔCp_{MAT} is the heat capacity variation of the fully amorphous tested material (which could be PLA or any of its nanocomposites). These values were obtained as described above in Section 2.3.2 by DSC. $\Delta Cp'$ is the specific heat change of the specimen (PLA or any of its composites) in a completely amorphous state at its particular T_g, while ΔCp is the specific heat change of the same specimen under test conditions (solvent-cast or isothermal crystallization) at its corresponding T_g. In order to acquire an accurate value for Cp, a representative point and a representative slope were considered before and after the T_g. From these values two equations were obtained, one that extrapolates the value of Cp before the glass transition and the other, which extrapolates the value after the glass transition. The ΔCp was calculated as the difference between both values (using the corresponding T_g for each crystalline morphology).

The RAF was calculated by means of Eq 3:

$$\% \, RAF = 100 - \% \, MAF - \%X_c - X_{nano} \, (Eq \, 3)$$

where RAF is the rigid amorphous fraction, MAF the mobile amorphous fraction, X_c the degree of crystallinity, and X_{nano}, nanoparticle content (wt%).

Finally, the RAF was separated between the RAF_{NANO} (induced by nanoparticles) and RAF_{CRYST} (induced by crystallinity, as has also been done for PLA/nanoclay nanocomposites [36]. First, the RAF_{NANO} was calculated by means of Eq 4 (the heat capacity variation among fully amorphous PLA and fully amorphous composites is due to RAF and nanoparticles) and afterwards the value of RAF_{CRYST} was calculated by means of Eq 5.

$$\% \, RAF_{NANO} = \left(1 - \frac{\Delta Cp_{MAT}}{\Delta Cp_{PLA}} - X_{nano}\right) * 100 \, (Eq \, 4)$$

$$\% \, RAF = \%RAF_{NANO} + \%RAF_{CRYST} \, (Eq \, 5)$$

In Eq 5, ΔCp_{PLA} is the heat capacity variation of fully amorphous PLA, while ΔCp_{MAT} is the heat capacity variation of the fully amorphous tested material.

Data from isothermal crystallization experiments within the range 10-70% relative crystallinity were fitted to the Avrami kinetic model [37] (Eq 6):

$$\ln\left(-\ln(1-X_c)\right) = \ln k + n \times \ln t \, (Eq \, 6)$$

251

252 In Eq 6, X_c is the relative degree of crystallinity, k is the overall kinetic constant, n is the Avrami index, and t is

253 crystallization time. The start time (t_0) was considered the time at which crystallization was noticeable (therefore

254 right after t_{delay}). The Avrami indeces are based on two factors (Eq 7), namely the growth directions of the

255 spherulites (n_D), which is a value ranging from 1-3 that is dependent on the growth directions of the spherulites,

256 and the time-dependent crystallization (n_N), which has a value between 0 for instantaneous nucleation and 1 for

257 sporadic nucleation [37].

258
$$n = n_D + n_N \text{ (Eq 7)}$$
259

260 ### 2.3.4 XRD

261 Isothermal crystallization was also measured by XRD using a Philips X'Pert Pro diffraction system fitted with

262 an Anton Paar HTK 1200N oven chamber and utilizing a Cu-tube ($\lambda = 1.542$ Å) operating at 40 kV and 40 mA.

263 A heating/cooling profile similar to that described in Figure 1 for DSC was used; however, due to cooling

264 restrictions, the samples were only cooled to 50°C instead of 0°C. During the isothermal crystallization stage,

265 diffraction patterns were acquired with a scan range of 10-30 °2θ, step size of 0.067° and acquisition time of 1

266 min. After completion of the isothermal crystallization procedure the samples were cooled to 50°C, at which

267 point an XRD pattern was acquired over the same scan range, but with a smaller step size of 0.017 and longer

268 acquisition time of 10 min to enhance the signal/noise ratio.

269

270 The solvent-cast materials, the amorphous materials (after hot pressing/quenching) and isothermally crystallized

271 materials (hot pressed and crystallized in an oven) were analyzed by the same XRD instrument at room

272 temperature, but without the oven chamber and using scan range of 10-30 °2θ, step size 0.04° and 4 s/step.

273

274 ### 2.3.5 Optical properties by UV-Vis spectroscopy

275 Optical properties were measured from at least three different points within the same sample under investigation

276 using a UV-Vis spectrometer (Polar Star Omega) in the range of 200-1000 nm. An average of the measurements

277 is presented.

278

279 ## 3. RESULTS AND DISCUSSION

280

281 ### 3.1 Discussion on material preparation

282 One of the key parameters for the successful improvement of properties in nanocomposites is to achieve good

283 nanoparticle dispersion. In the present work, PLA was reinforced with two different nanoparticles of different

284 nature (one hydrophilic, CNF, and one hydrophobic, C30B) and thus each behaves differently in the same

285 solvent. It was not possible to find a common solvent/procedure, which led to both particles being well-

286 dispersed and possessing suitable film properties. Therefore, to ensure a good dispersion of nanoparticles in the

287 composites and thus allow a fair comparison, the best solvent and processing procedure (the ones that they were

288 leasing to better nanoparticle dispersion) for each nanoparticle was used in each case. For C30B it was found

289 that use of DCM as solvent followed by drying at room temperature led to well- dispersed composites with good

290 film quality, whereas the same procedure applied to CNF led to poorly dispersed composites. After evaluation

291 of different solvents, it was found that DMF was the most suitable solvent for this particular CNF, and that 80°C

292 was the best drying temperature. As summarized in Table 1, all composites were prepared with 1 wt% of
293 nanoparticles, in order to strike a balance between a good dispersion and a significant increase in material
294 performance, while minimizing the chance of clay platelet/nanofiber aggregates being present.

295 **Table 1 Composition of the samples; PLA and nanocomposites in wt%.**

	PLA	CNF	C30B
PLA	100%	-	-
PLA/C30B	99%	-	1%
PLA/CNF	99%	1%	-
PLA/CNF/C30B	98%	1%	1%

296 The CNF shows a diameter of 27 +/-13 nm and a length of 658 +/- 290 nm and is well dispersed in the
297 nanocomposites as reported elsewhere. [10,2] The montmorionite-based C30B in the PLA/C30B and hybrid
298 composites is also well dispersed, near to full-exfoliation[5] and is therefore approximated to have individual
299 layers of 400 x 300 x 1 nm[11].
300

301 3.2   **Spherulite morphology and distribution by POM**
302 The spherulite morphology and distribution in PLA and PLA nanocomposites prepared by solvent casting,
303 followed by complete isothermal crystallization at 100°C, 120°C and 140°C, were evaluated by POM (see
304 **Error! Reference source not found.**). First, the differences between solvent casting and isothermal
305 crystallization were investigated. Solvent-cast samples (Figure 2, first row) of PLA/CNF and PLA/CNF/C30B
306 show micron-sized (around 40 µm) spherulites, while any spherulites present in PLA and PLA/C30B are too
307 small to be observed by POM, though DSC shows a crystallinity of 7 and 32% respectively in these samples.
308 Furthermore, the presence of C30B does not influence the spherulite nature when combined with CNF. Though
309 crystallization has occurred in the CNF-containing samples (34 and 35%, respectively, according to DSC) the
310 spherulites do not cover the whole area.

311 It is clear that spherulite size is not only a result of the type of reinforcing agent, but is also highly dependent on
312 the processing conditions, illustrating that processing temperature is a key factor for spherulite size and
313 distribution.
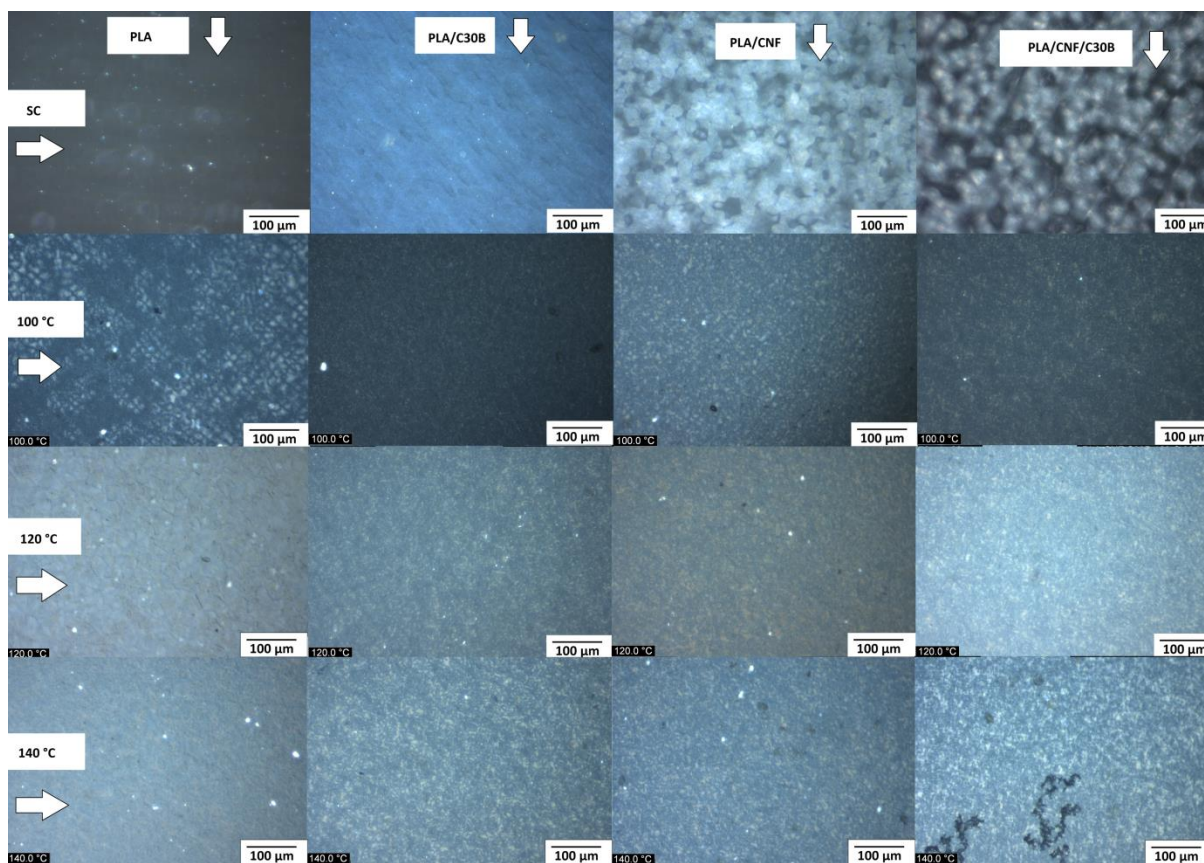
Figure 2 POM of PLA and nanocomposites (1wt% per nanoparticle type) with different crystalline morphologies. 1st row) Solvent cast, 2nd row) crystallized at 100°C, 3rd row) crystallized at 120°C) and 4th row) crystallized at 140°C.

When comparing the fully crystallized morphologies between the isothermally crystallized nanocomposites at different crystallization temperatures (Figure 2, rows 2-4 and columns 3-4) no clear differences are observed, but there is a large difference when comparing these with the respective PLA samples (Figure 2, rows 2-4, column 1, inclusively). The nanocomposites, at all crystallization temperatures, show a greater amount of much smaller and more evenly distributed spherulites resulting from nucleation caused by the CNF and C30B that are homogeneously distributed, whereas the PLA contains larger spherulite sizes (up to ~65 μm) that are heterogeneously distributed. Evaluating the crystalline morphology of the fully crystallized samples is complicated due to the high amount and close packing of spherulites. But POM photographs of PLA and its nanocomposites taken at an earlier stage of the isothermal crystallization (approximately 20-30% of the total crystallization at 120°C, Figure 3) allows some differentiation. Here, it can again be seen that PLA contains much larger spherulites, whereas all of the nanocomposites contain substantially smaller homogeneously distributed spherulites because of the nucleating properties of the nanoparticles.
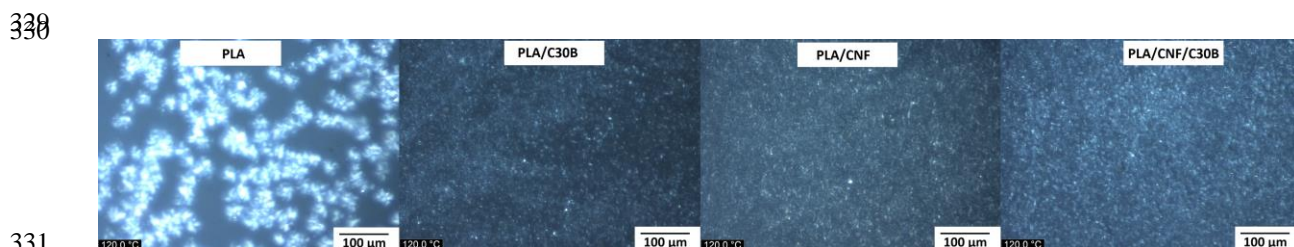
Figure 3 POM of PLA and its nanocomposites (1 wt% per nanoparticle type) during crystallization at 120°C.

3.3   XRD studies

10

In order to elucidate which crystalline phase is generated by different crystallization procedures, and whether the nanoparticles could induce the formation of one phase over another, XRD patterns were collected. There are two thermally induced phases, α (ordered) and α´ (disordered) and it has already been reported that lower processing temperatures tend to favor the creation of the disordered phase [23]. To aid investigation and for comparison, XRD patterns were also collected at 80°C, since this was likely to be a relevant temperature to observe the formation of the α´ phase. The α and α´ phases can be distinguished, since the latter does not exhibit any characteristic peaks, such as those corresponding to reflection plane 210, which is located at 2θ ~ 22.5°, while the peaks that are present in both phases, such as 200/110 and 203/113, are shifted to lower 2θ angles in the α´ phase [23,34].
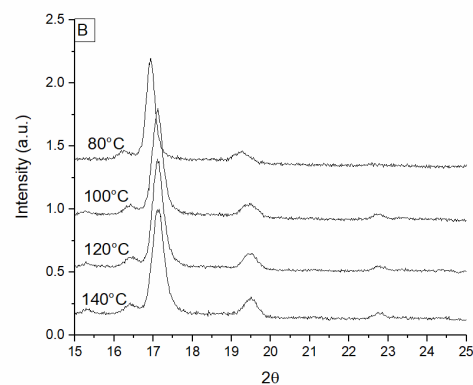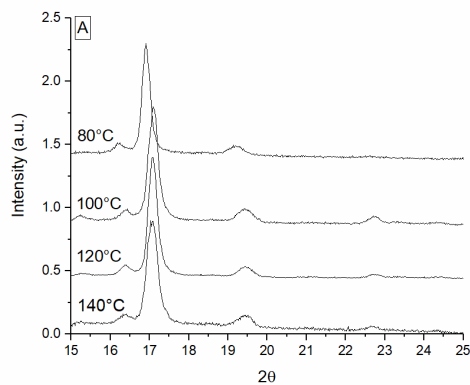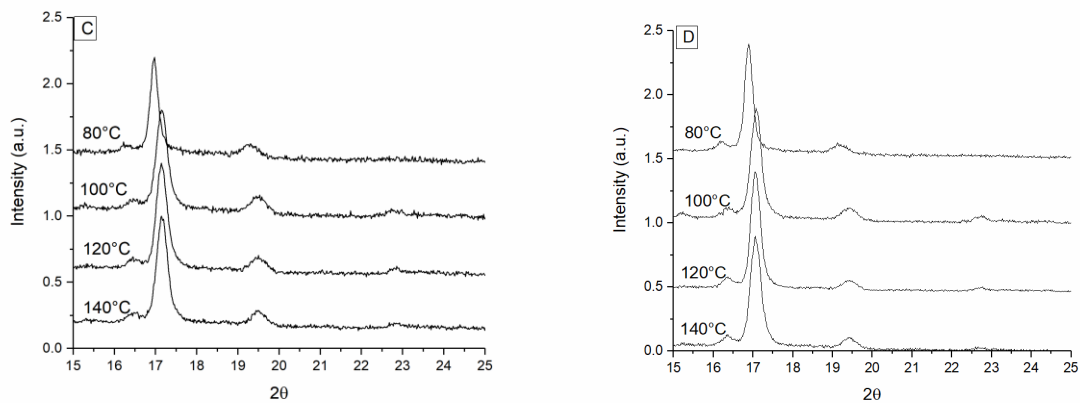
Figure 4 presents the XRD patterns collected from isothermally crystallized PLA and its nanocomposites. In the left column are the two main crystallinity peaks of PLA at $2\theta \sim 17°$, which corresponds to the reflection planes 200/110, and $2\theta \sim 19.5°$, which corresponds to plane 203/113. While no significant variations in the relative positions of these peaks were observed in the solvent-cast nanocomposites due to the addition of different nanoparticles (Figure 4B-C), it was found that the crystallization temperature was clearly affecting peak position. There is a shift to lower 2θ (~0.2°) when comparing samples crystallized at >100°C with samples crystallized at 80°C, this shift, as mentioned above, has been associated to α´ phase. It can be also seen that the peak at 2θ ~22.5°, corresponding to reflection plane 201, and which is associated with the α phase, is present in the PLA and nanocomposites crystallized at 140°C, 120°C, and 100°C, while it is completely absent in the PLA and nanocomposites crystallized at 80°C. This supports the conclusion that PLA and nanocomposites crystallized at 80°C contain predominantly the α´ phase, while nanocomposites crystallized at higher temperatures predominantly contain the α phase.

In order to evaluate whether the solvent casting procedure also induces the α´ phase, the XRD patterns (Figure 5) of the solvent-cast (SC) PLA and nanocomposites were compared with those of the respective fully amorphous (AM - obtained from hot pressing at 170°C followed by fast quenching) and fully crystallized (FC (120°C)) - fully amorphous composites that were thereafter crystallized for 120 mins at 120°C in an oven) samples. Note that the XRD patterns in Figures 4 and 5 are not directly comparable because the former were collected during a crystallization monitoring experiment at 50°C (due to cooling restrictions) while the patterns in Figure 5 were collected at room temperature. Although the intensities may differ, the peak positions remain comparable.

12

376

377

378
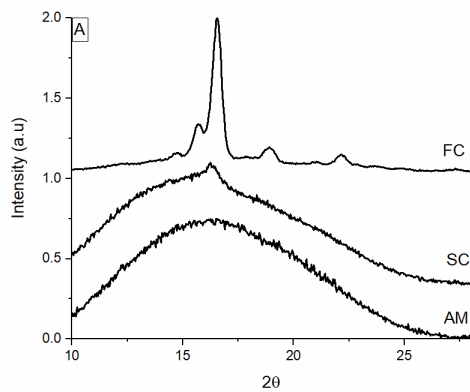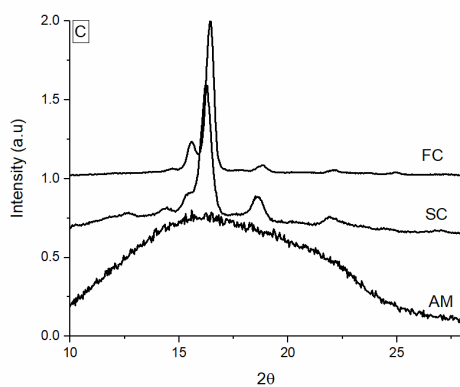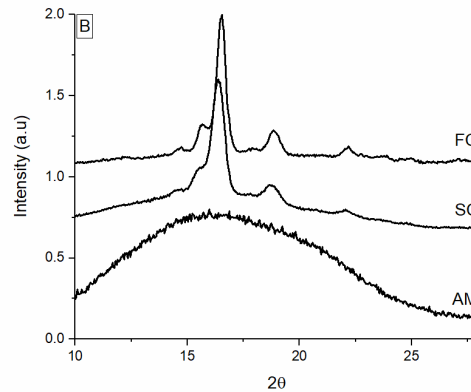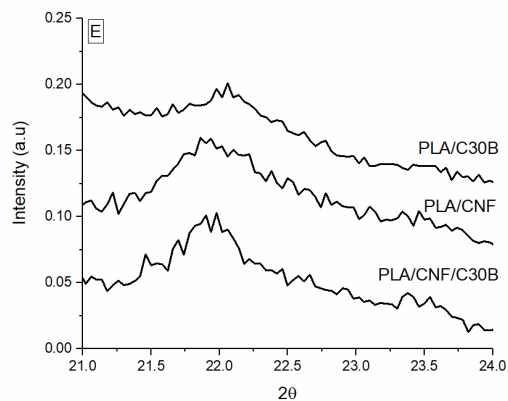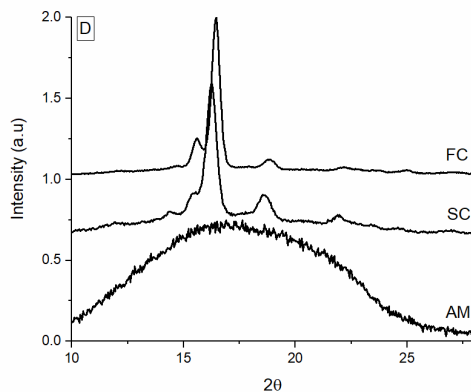
Figure 5 XRD patterns of solvent cast, amorphous and fully crystallized materials. From A) to D) same material under different crystalline morphologies; A) PLA, B) PLA/C30B, C) PLA/CNF, D) PLA/CNF/C30B. E) Zoom-in of all of the solvent cast materials in the range of $2\theta = 21\text{-}24$. All of the composites have a 1wt% of each nanoparticle type.

It is noticed that there is also the same shift to lower 2θ for all of the two main crystallinity peaks for the solvent-cast samples when compared with those crystallized at 120°C which contained mainly the α phase; therefore, it can also be concluded that the solvent-cast samples contained mainly the α´ phase. However, in Figure 5E it can be seen that all of the diffraction traces from the solvent-cast nanocomposite samples, especially the PLA/CNF and PLA/CNF/C30B, also showed a small peak at $2\theta \sim 22°$, which is ascribed to the α

phase. In fact, other researchers [38] have discussed the formation of the α-phase in solvent-cast samples even at low temperature, due to an increase on chain mobility arising from the solvent. However, in the present work there is apparently a coexistence of both phases. The α-phase is attributed to the solvent casting itself, while the α´-phase is attributed to the drying of the materials after solvent casting, at temperatures below the α-phase formation temperature ($< 80°C$).

It is reassuring to note that no crystalline peaks were found for the fully amorphous (AM) quenched composites, but only a broad characteristic amorphous halo, thereby proving that the procedure used to prepare hot-pressed amorphous samples (hot pressing at 170°C for 5 minutes) followed by fast cooling was successful.

3.4 Evaluation of the impact of nanoparticles on isothermal crystallization kinetics

The isothermal crystallization kinetics of PLA and its nanocomposites were monitored at 140°C, 120°C, 100°C and 80°C, the results are presented in Table 1 except for PLA at 140°C, since crystallization was not complete, and for all of the samples at 80°C since the rate was too slow to determine.

Table 2 Half-crystallization and crystallization detection times of PLA and composites.

T (°C)	PLA t_{delay}[a]	PLA $t_{1/2}(exp)$[b]	PLA/C30B t_{delay}[a]	PLA/C30B $t_{1/2}(exp)$[b]
140			0.5	11.5
120	2.4	26	0.4	2
100	4.9	52.1	1.8	3.7

T (°C)	PLA/CNF t_{delay}[a]	PLA/CNF $t_{1/2}(exp)$[b]	PLA/CNF 1%/C30B t_{delay}[a]	PLA/CNF 1%/C30B $t_{1/2}(exp)$[b]
140	2.7	30.8	2.2	25.2
120	1.8	10.3	0.8	4.8
100	2.9	24.5	3.4	15.2

a) t_{delay} (delay from arrival to the crystallization temperature and the start of the peak in DSC,
b) $t_{1/2}$ half-crystallization time (since the sample reached crystallization temperature)

The crystallization rate reach a maximum at 120°C for all samples, and it is evident that the nanocomposites crystallize faster than neat PLA at the investigated temperatures. Among the nanocomposites, PLA/C30B showed faster nucleation than PLA/CNF or PLA/CNF/C30B, which was even more pronounced at 140°C. The better performance of C30B as a nucleating agent compared with CNF could be explained by the fact that clay is more likely to have a higher specific surface area, resulting in an increasing number of nucleation sites. In general, it was also found that t_{delay} (the time between the material reaching the crystallization temperature and onset of the crystallization peak) was proportional to the half-crystallization time.

In order to retrieve more information regarding crystallization kinetics, data from isothermal crystallization experiments within the range of 10-70% relative crystallinity were fitted to the Avrami kinetic model as described in materials and methods, resulting in the Avrami indeces shown in Table 3.

T (°C)	PLA	PLA/C30B	PLA/CNF	PLA/CNF/C30B
140		1.52	1.94	2.12
120	1.97	1.73	1.91	2.43
100	2.27	2.36	1.99	2.49

417 PLA/C30B nanocomposite showed a strong tendency to decrease the Avrami indeces, in line with increased
418 crystallization temperature reflecting decreased growing directions. A similar trend has also been reported by
419 other authors for PLA[39], and PLA with 10% and 15% of C30B [40] and PLA with other organically modified clays
420 at 1% and 3% loading [41]. There are also other reports claiming a more moderate trend [42], which might be
421 attributed to differences in clay dispersion. Notwithstanding this point, the PLA/CNF nanocomposite had
422 constant values regardless of crystallization temperature, which is in agreement with some reports in the
423 literature for low bacterial cellulose content in PLA [43] and for non-modified nanocrystalline cellulose in PLA [44].
424 Interestingly, it was found that the hybrid nanocomposite PLA/CNF 1%/C30B 1% showed moderate variation
425 in Avrami indices in line with increasing temperature between that of CNF and C30B, thereby suggesting the
426 simultaneous growth of both clay- and nanocellulose-nucleated spherulites. In any case, all of the composites
427 showed no major dissimilarities in values of n suggesting that there is no strong effect from the nanoparticles on
428 the spherulite growing direction. Avrami indeces for the neat PLA (n=1.97 for crystallization at 120°C and
429 n=2.27 for crystallization at 100°C) were not considered because, as can be seen in **Error! Reference source**
430 **not found.**, after complete crystallization at 120°C, the PLA spherulites reached a diameter of approximately 65
431 μm, while PLA film showed a thickness of 75 μm. Consequently, a spherulite growing in PLA could be affected
432 by the physical dimensions of the film.

433

434 **3.5**   **Influence of crystallization temperature and nanoparticles on thermal transitions**

435 The effect of the crystallization temperature and the presence of nanoparticles on T_g and T_m was studied by
436 DSC, and the results are shown in Table 4. PLA is known to have a very low T_g, which limits it performance in
437 some areas such as packaging of microwave-heated food or hot tea-coffee cups among others. Additionally, a
438 large variation on T_m will certainly affect the optimal PLA processing temperature in an extruder during
439 thermoforming. This is relevant for PLA, but it is critical for PLA/CNF composites since cellulose and CNF
440 suffer from degradation at high temperature. Therefore, an evaluation of the impact of the nanoparticles and
441 nanoparticle- induced crystallization is fundamental to optimize the performance of the composites.

442

Crystallization	PLA		PLA/C30B		PLA/CNF		PLA/CNF/C30B	
	T_g	T_m	T_g	T_m	T_g	T_m	T_g	T_m
140°C[a]	58.8	162.3	57.6	161.9	56.5	163.2	57.9	162.6
120°C[a]	61.7	154.9	58.8	154.4	60.0	155.3	59.6	154.4
100°C[a]	60.5	149.4	61.9	149.3	61.2	150.6	62.0	150.3

Amorphous[c]	55.5	-	56.2	-	54.9	-	55.2	-
SC[b]	60.4	155.0	59.8	154.5	61.7	151.1	61.4	153.7

445   a) Isothermal crystallization at the corresponding crystallization temperature.
446   b) Solvent-cast nanocomposites: PLA and PLA/C30B at 23°C; PLA/CNF and PLA/CNF/C30B at 80°C.
447   c) Amorphous nanocomposites obtained from a fast melt-quenching.

448   In general, the incorporation of CNF and/or C30B did not have a significant impact on the T_g or T_m of PLA
449   within the respective isothermally crystallized samples; however, the T_m of all of the PLA and nanocomposite
450   samples did increase in line with increased crystallization temperature. For example, when increasing the
451   isothermal crystallization temperature of PLA from 100 to 140°C, the T_m increased from 149.4 to 162.3°C,
452   whereas for PLA/CNF 1% it increased from 150.6 to 163.2°C. The reason of this increased melting temperature
453   with increases crystallization temperature is that at high temperatures larger, more stable, lamellae are formed
454   within the spherulites which melt at higher temperatures It can also be seen that all of the isothermally
455   crystallized materials showed higher T_g values when compared with the respective amorphous materials, which
456   is attributed to a constriction of the MAF occurring after the material is crystallized. However, this might not be
457   a direct effect of the crystallinity, but is probably due to induced changes on the amorphous region by the
458   growing spherulites. The MAF trapped between spherulites has also been shown to have different relaxation
459   values when compared with the amorphous matrix [36]. In this context, the presence of nanoparticles, unlike
460   crystallization, does not constrain the amorphous phase as much as the presence of spherulites otherwise a larger
461   variation would be observed between the T_g values of neat PLA and PLA nanocomposites. Finally, it was found
462   that the T_m values of the solvent-cast PLA/CNF (151.1°C) and PLA/CNF/C30B (153.7°C) were slightly below
463   the values of solvent-cast PLA (155.0°C) and PLA/C30B (154.5°C), suggesting that the different crystalline
464   morphology for these two groups of samples, as observed in **Error! Reference source not found.**, have a small
465   impact on T_m; however, variations among the materials are close to the accuracy of the DSC.

466   ### 3.6   Crystallinity and mobile/rigid amorphous fraction

467   It is widely accepted that crystallinity plays a very important role in materials properties, which makes
468   crystallinity analysis (usually by DSC) essential for evaluation of the properties of materials and composites.
469   Recently, evaluation of the so-called Rigid Amorphous Fraction (RAF) and its impact on material properties has
470   been receiving additional attention. Apart from reducing the Mobile Amorphous Fraction, (MAF), which are the
471   only "mobile" domains, and therefore essential for the extensibility of the material, it has been speculated that
472   the RAF could be linked to specific material properties. Among other factors, the RAF is suspected of having a
473   larger free volume than the MAF, which would have a significant impact on the sorption properties of the
474   material. Therefore, understanding how crystallization affects those properties could be key to understanding,
475   foreseeing and optimizing material properties.

476

477   The melting enthalpy of 100% α-crystalline PLA was considered to be 106 J g^{-1}, while that of 100% α'-
478   crystalline PLA was considered to be 25 J g^{-1} lower at 81 J g^{-1} [34], while for solvent-cast materials an
479   intermediate value of 93 J g^{-1} was used (average of the enthalpy of the α and α' phases). The heat capacity
480   change at the T_g of fully amorphous PLA was found in this study to be 0.55 J g^{-1} K^{-1}, which is similar to what
481   has been found by others, between 0.48 and 0.628 J g^{-1} K^{-1} [34,35,45,46]. As expected, The heat capacity variation at

the glass transition temperature of the fully amorphous nanocomposites are slightly lower than the neat PLA and are shown in Error! Reference source not found.. Additionally, in the same Table, the values of RAF induced by nanoparticles (RAF_{NANO}) are presented as calculated by means of Eq 4. The values of the heat capacity of PLA and nanocomposites at the T_g can be found in the supplementary information (Table S1).

Furthermore, the MAF and RAF values of the PLA and its nanocomposites alongside their degrees of crystallinity are summarized in Table 5. RAF values in Table 4 have been split according to RAF induced by the crystalline morphology (RAF_{CRYS}) and the total RAF (i.e. RAF_{CRYS} + RAF_{NANO}) by means of Eq 4. The completely amorphous PLA/C30B 1% sample has a RAF of 4%, which therefore defines the RAF_{NANO} as 4%, since there is no impact from crystallinity. The solvent-cast PLA/C30B 1% sample has a RAF (i.e. total CRYS + NANO) of 16%, while 4% of this is the RAF_{NANO} (same as the amorphous sample) and the remaining 12% is attributed to RAF_{CRYS}.

Table 5 Degree of crystallinity (X_c), mobile amorphous fraction (MAF), and rigid amorphous fraction (RAF) of PLA and nanocomposites under different crystalline morphologies.

Isothermal Crystallization	PLA			PLA/C30B		
	X_c	MAF	$RAF/RAF_{CRYS}/RAF_{NANO}$[d]	X_c	MAF	$RAF/RAF_{CRYS}/RAF_{NANO}$[d]
140°C[a]	--	--	--	36%	43%	20%/16%/4%
120°C	35%	42%	22%	39%	36%	24%/20%/4%
100°C	33%	45%	23%	36%	36%	27%/23%/4%
Amorphous[c]	0%	100%	0%	0%	95%	4%/0%/4%
SC[b]	6%	90%	4%	29%	54%	16%/12%/4%
Isothermal Crystallization	PLA/CNF			PLA/CNF/C30B		
	X_c	MAF	$RAF/RAF_{CRYS}/RAF_{NANO}$[d]	X_c	MAF	$RAF/RAF_{CRYS}/RAF_{NANO}$[d]
140°C	36%	43%	20%/16%/4%	37%	37%	24%/15%/9%
120°C	37%	38%	24%/20%/4%	40%	32%	25%/16%/9%
100°C	36%	37%	26%/22%/4%	37%	33%	28%/19%/9%
Amorphous[c]	0%	95%	4%/0%/4%	0%	89%	9%/0%/9%
SC[b]	34%	41%	29%/25%/4%	35%	35%	32%/23%/9%

a) The data for PLA at 140°C are not presented, due to incomplete crystallization.
b) Solvent-cast nanocomposites: PLA and PLA/C30B at 23°C; PLA/CNF and PLA/CNF/C30B at 80°C.
c) The amorphous nanocomposites were obtained from a fast melt-quenching.
d) Rigid amorphous fraction: Overall RAF%/% /RAF_{CRY}/RAF_{NANO}).

504 Regarding the presence of nanoparticles, seemingly both CNF and C30B showed a similar impact on the
505 formation of RAF_{NANO} in amorphous samples (each at 4%), despite the fact that C30B is likely to show a higher
506 specific area than CNF. This is attributed to the presence of the long chain hydrophobic modifier present on the
507 C30B surfaces apparently minimizing the creation of RAF_{NANO} by enhancing compatibility between polymer
508 matrix and nanoparticles. Hybrid CNF/C30B showed an RAF_{NANO} (9%) close to the combination of the
509 RAF_{NANO} induced by the two types of particles individually. A corresponding decrease in MAF is observed
510 when C30B or CNF is added and suggests the nanoparticles are well dispersed and do not interact with each
511 other, since interaction among nanoparticles is likely to decrease the overall surface area of nanoparticles in the
512 polymer matrix and lead to a decreased RAF.

513 The RAF of neat PLA isothermally crystallized at 100°C (23%) and 120°C (22%) is in the higher range of
514 values presented in the literature (12%-22%) [35,36,47]. When evaluating the effect of isothermal crystallization
515 temperature on the RAF values for all samples it can be noted that higher crystallization temperature leads to
516 slightly reduced RAF, which is a trend reported in the literature [48].

517 It is shown that all of the isothermally crystallized and solvent-cast nanocomposites exhibit increased
518 crystallinity and a reduced MAF when compared with the respective neat isothermally crystallized PLA
519 samples. This is considered a result of the smaller spherulite sizes induced in nanocomposites (Figure 2),
520 allowing for a better packing of the different spherulites within the matrix, which subsequently allowed the
521 formation of more crystalline domains, thus decreasing the MAF. The isothermally crystallized nanocomposites
522 showed an increased $RAF_{CRYS+NANO}$, compared to neat PLA, which was due to the presence of nanoparticles.
523 When comparing the values of RAF_{CRYS} it can be seen that the nanocomposites have lower values. Furthermore,
524 it can be observed that solvent-cast PLA/C30B 1% shows a much lower amount of RAF (13%) than solvent-cast
525 PLA/CNF 1% (25%) and solvent-cast PLA/CNF 1% (28%). This combined with the fact that the former has a
526 much smaller spherulite size (as shown in Figure 2 - top row) and the extent of crystallinity for all three samples
527 is approximately the same, suggests that spherulite size and RAF are closely related.

528 **3.7   Evaluation of the influence of crystalline morphology and nanoparticles on optical transparency**

529 The impact of nanoparticles and crystalline morphology on the transparency of films was investigated, and the
530 results are summarized in Figure 6. Transparency is a key property in plastics for food packaging applications,
531 and while nanoparticles are smaller than the wavelength of the visible light and therefore should not influence
532 the transmission of visible light, their impact on crystallinity might affect transparency.
533

534

535
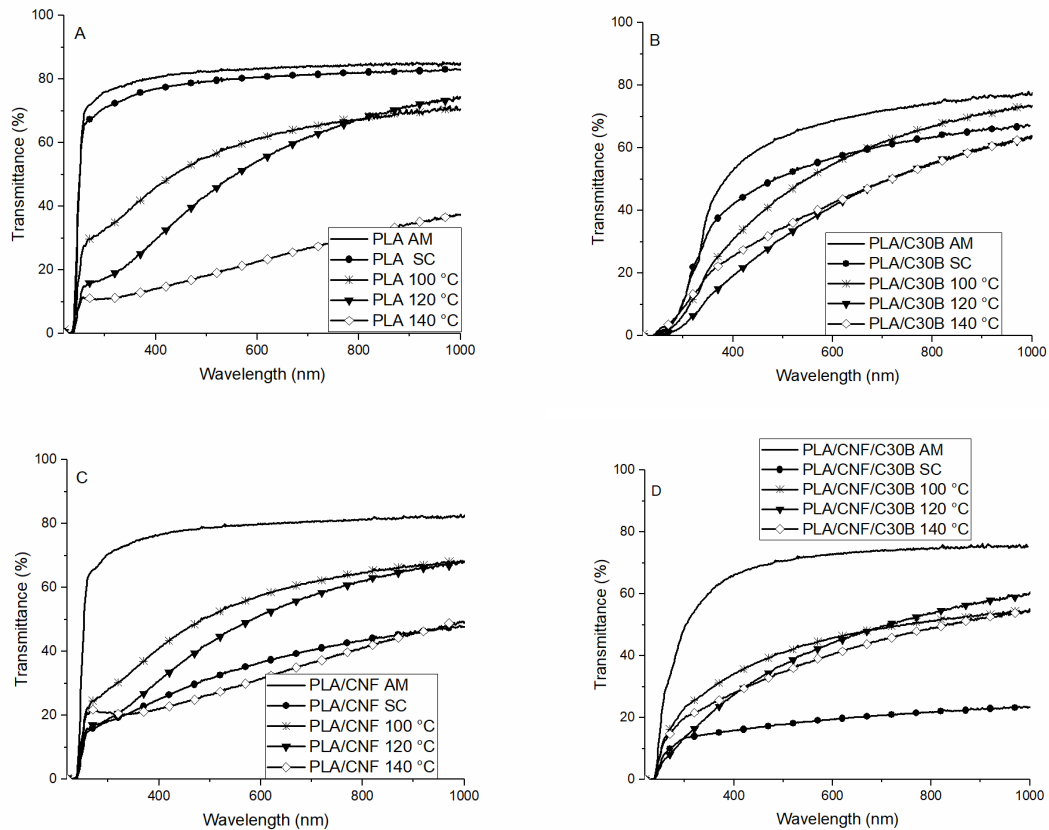
Figure 6 UV-VIS spectra of neat PLA and its nanocomposites with different crystalline morphologies after isothermal crystallization at different temperatures, and for amorphous- and solvent casting-induced crystallinity.

When evaluating the impact of crystallization temperature on the transparency of films, it is evident that crystallization at 100°C leads to more transparent materials, although the difference in materials crystallized at 120°C is generally small. Surprisingly, crystallization at 140°C dramatically affects the transparency of PLA and CNF-containing nanocomposites, whilst not having such a significant influence on nanocomposites with C30B. Assuming that there is no noticeable change in crystalline morphology among PLA/CNF, PLA/C30B and PLA/CNF/C30B crystallized at 140°C, and also that PLA shows incomplete crystallization at this temperature, this effect is mostly attributed to a temperature-induced internal deformation (i.e. bubbles or irregularities), which can cause light scattering.

This observation is interesting, assuming that the decrease in transparency is due to thermal deformation, it is anticipated that composites showing better thermomechanical properties would provide better transparency. Higher thermomechanical resistance leads to less deformed material. However it could be argued that there is an inconsistency with PLA/CNF crystallized at 140°C, material that in our previous work [2] showed better thermomechanical properties than PLA/C30B but still showed reduced transparency without any clear difference in crystalline morphology. However, this can be explained based on the different reinforcing mechanisms of both nanoparticles. Previously we have observed better reinforcing performance of CNF, which was attributed to the establishment of a percolated network of the CNF, which can uphold any stress of the polymer chains. Meanwhile, the higher specific area and higher compatibility of C30B should lead to stronger interfacial bonding between the polymer matrix and the clay (including the aliphatic chains at its surface) and

19

556 thus allows a better stress transfer. This anchoring mechanism of the chains by the nanoclays, also reported

557 elsewhere [36], prevents any shape degradation during the higher temperature processing and reduces any thermal

558 deformation as observed with CNF. In the case of CNF, care should therefore be taken during processing, since

559 too high a processing temperature could lead to reduced performance. Presumably, in this scenario the reduced

560 surface area of CNF and lower compatibility with the polymer matrix leads to deformations at higher processing

561 temperatures due to a lack of anchorage between polymer chains and nanoparticles.

562 When comparing respective amorphous samples with nanocomposites isothermally crystallized at 120°C and

563 100°C, it is evident that, for all of the cases, increased crystallinity leads to reduced transparency in the visible

564 region of the spectra (>400 nm). This can be explained by the fact that crystalline domains have higher density

565 than amorphous domains, which leads to light scattering as the light passes between each of the domains. It is

566 also noteworthy that the presence of nanoparticles does not significantly affect the transparency of films within

567 the isothermally crystallized samples, which is presumably due to the dispersion of the nanoparticles on a

568 nanometer scale. A similar observation can be seen for the respective amorphous nanocomposites, although in

569 this case the PLA/C30B does show a slight decrease in transparency. When evaluating the transparency of

570 solvent-cast films, it can be seen that solvent-cast PLA/C30B shows increased transparency when compared to

571 the other nanocomposites, while PLA/CNF/C30B shows a significantly reduced transparency. This is attributed

572 to smaller or larger spherulite sizes observed in the solvent-casted PLA/C30B or PLA/CNF/C30B

573 nanocomposites as shown in Figure 2 (row 1). In addition to this, also the amount of RAF could affect the

574 transparency of the samples. RAF has been reported to have a larger free volume than the MAF,[49] which

575 ultimately could cause light scattering and effectively the free volume regions of RAF could act as "bubbles" in

576 a polymer matrix.

577 A UV-blocking effect (reduction of transmittance below 400nm) can be seen for PLA/C30B 1%, which is not

578 observed for PLA/CNF 1% which shows behavior similar to PLA. Surprisingly, PLA/CNF 1%/C30B 1% shows

579 less of a UV-blocking behavior when compared with PLA/C30B 1%, even though the same amount of C30B is

580 present. A better dispersion of clay (i.e. exfoliation) will lead to increased nanoparticle surface area that can

581 block UV light [50] suggesting this effect may be attributed to small differences in clay dispersion between C30B-

582 reinforced composites caused by the presence of CNF. It is remarkable that, after full crystallization, at any of

583 the temperatures studied, the hybrid nanocomposites containing 1% CNF and 1% C30B shows good

584 transparency, which is often a desirable feature for food packaging films.

585 **4. CONCLUSIONS**

586

587 In the present work, the influence of processing conditions on the crystallinity of solvent-cast and isothermally

588 crystallized PLA, PLA/CNF 1%, PLA/C30B 1%, and PLA/CNF 1%/C30B 1% was evaluated by DSC, MDSC,

589 POM, and XRD. It was found that solvent casting at room temperature induces a different crystallinity

590 compared to isothermal crystallization and therefore leads to materials with different performance compared to

591 high temperature processed materials. Similarly, composites prepared at high temperature, might not accurately

592 be used to assess material properties, when the material ultimately is intended to be processed via solvent-based

593 electrospinning at lower temperatures. However, different solvent casting methods were shown to induce

different crystallinity. The combination of both CNF and C30B did not show significant variations in spherulite size or distribution when compared with single nanoparticle- filled composites.

The thermal transitions were not significantly influenced by the nanoparticles, but the increasing isothermal crystallization temperatures did result in decreasing glass transition temperature and increasing melting points when assessing nanoparticles either individually or in combination. The kinetic investigation of crystallization demonstrated that combining both types of nanoparticles did not lead to a sum of both crystallization rates but to an average. A similar effect was also observed with spherulite growth directions. PLA/C30B 1% showed a clear tendency towards decreased growing directions with increased crystallization temperature, whereas PLA/CNF 1% showed no significant variations and a combination with PLA/CNF 1%/C30B 1% showed only a moderate intermediate decrease in growing direction. The combination of both nanoparticles within the amorphous matrix effectively led to a doubling of the RAF_{NANO}, which was also due to the sum of each individual nanoparticle; however, no further variations in RAF_{NANO} due to the effect of each nanoparticle was apparent after full isothermal crystallization. Within the isothermally crystallized samples, the main difference in the hybrid composites was a reduced MAF, which was compensated by an increase in extent of crystallinity, probably due to better spherulite packaging.

Transparency of the nanocomposites generally depended on the spherulite size, which was clearly seen for the solvent casted samples. For isothermally crystallized samples, a similar degree of crystallinity and spherulite size were determined, though higher crystallization temperatures resulted in lower transparency, which was attributed to defects in the materials rather than crystallization phenomena.

5. ACKNOWLEDGEMENTS

6. Data availability

The raw and processed data required to reproduce these findings cannot be shared at this time due to technical or time limitations

7. REFERENCES

1.   Madhavan Nampoothiri, K.; Nair, N. R.; John, R. P. *Bioresour. Technol.* **2010**, *101*, 8493.

2.   Trifol, J.; Plackett, D.; Sillard, C.; Hassager, O.; Daugaard, A. E.; Bras, J.; Szabo, P. *J. Appl. Polym. Sci.* **2016**, *133*, 1.

3.   Khalil, H. A.; Bhat, A. H.; Yusra, A. I. *Carbohydr. Polym.* **2012**, *87*, 963.

4.   Krishnamachari, P.; Zhang, J.; Lou, J.; Yan, J.; Uitenham, L. *Int. J. Polym. Anal. Charact.* **2009**, *14*, 336.

5.   Trifol, J.; Plackett, D.; Sillard, C.; Szabo, P.; Bras, J.; Daugaard, A. E. *Polym. Int.* **2016**, *65*, 988.

6.   Wu, C. N.; Saito, T.; Yang, Q.; Fukuzumi, H.; Isogai, A. *ACS Appl. Mater. Interfaces* **2014**, *6*, 12707.

7.   Jamshidian, M.; Tehrany, E. A.; Imran, M.; Jacquot, M.; Desobry, S. *Compr. Rev. Food Sci. Food Saf.*

634   **2010**, *9*, 552.

635   8.   Bitinis, N.; Verdejo, R.; Maya, E. M.; Espuche, E.; Cassagnau, P.; Lopez-Manchado, M. A. *Compos.*
636   *Sci. Technol.* **2012**, *72*, 305.

637   9.   Fukuzumi, H.; Saito, T.; Isogai, A. *Carbohydr. Polym.* **2013**, *93*, 172.

638   10. Trifol, J.; Sillard, C.; Plackett, D.; Szabo, P.; Bras, J.; Daugaard, A. E. *Cellulose* **2016**.

639   11. Ploehn, H. J.; Liu, C. *Ind. Eng. Chem. Res.* **2006**, *45*, 7025.

640   12. Gorrasi, G.; Anastasio, R.; Bassi, L.; Pantani, R. *Macromol. Res.* **2013**, *21*, 1110.

641   13. Picard, E.; Espuche, E.; Fulchiron, R. *Appl. Clay Sci.* **2011**, *53*, 58.

642   14. Sarasua, J. R.; Arraiza, A. L.; Balerdi, P.; Maiza, I. *Polym. Eng. Sci.* **2005**, *45*, 745.

643   15. Garlotta, D. *J. Polym. Environ.* **2001**, *9*, 63.

644   16. Guinault, A.; Sollogoub, C.; Domenek, S.; Grandmontagne, A.; Ducruet, V. *Int. J. Mater. Form.* **2010**,
645   *3*, 603.

646   17. Perego, G.; Cella, G. D.; Bastioli, C. *J. Appl. Polym. Sci.* **1996**, *59*, 37.

647   18. Suryanegara, L.; Nakagaito, A. N.; Yano, H. *Compos. Sci. Technol.* **2009**, *69*, 1187.

648   19. Naga, N.; Yoshida, Y.; Noguchi, K.; Murase, S. *Open J. Polym. Chem.* **2013**, *03*, 29.

649   20. Miyata, T.; Masuko, T. *Polymer.* **1998**, *39*, 5515.

650   21. Jandas, P. J.; Mohanty, S.; Nayak, S. K. *J. Therm. Anal. Calorim.* **2013**, *114*, 1265.

651   22. Sarasua, J. R.; Rodriguez, N. L.; Arraiza, A. L.; Meaurio, E. *Macromolecules* **2005**, *38*, 8362.

652   23. Zhang, J.; Tashiro, K.; Tsuji, H.; Domb, A. J. *Macromolecules* **2008**, *41*, 1352.

653   24. Wunderlich, B. *Prog. Polym. Sci.* **2003**, *28*, 383.

654   25. Adam, G.; Gibbs, J. H. *J. Chem. Phys.* **1965**, *43*, 139.

655   26. Trifol, J.; Mericer, C.; Plackett, D.; Sillard, C.; Minelli, M.; Hassager, O.; Daugaard, a E.; Bras, J.;
656   Giacinti, M.; Szabo, P. *20th Int. Conf. Compos. Mater. Copenhagen* **2015**, 19.

657   27. López-Rubio, A.; Lagarón, J. M.; Hernández-Muñoz, P.; Almenar, E.; Catalá, R.; Gavara, R.; Pascall,
658   M. A. *Innov. Food Sci. Emerg. Technol.* **2005**, *6*, 51.

659   28. Martínez-Sanz, M.; Olsson, R. T.; Lopez-Rubio, A.; Lagaron, J. M. *J. Appl. Polym. Sci.* **2012**, *124*,
660   1398.

661   29. Mohanty, S.; Larsen, L. B.; Trifol, J.; Szabo, P.; Burri, H. V. R.; Canali, C.; Dufva, M.; Emnéus, J.;
662   Wolff, A. *Mater. Sci. Eng. C* **2015**, *55*, 569.

663   30. Mohapatra, A. K.; Mohanty, S.; Nayak, S. K. *Polym. Compos.* **2012**, *33*, 2095.

664   31. Katiyar, V.; Gerds, N.; Koch, C. B.; Risbo, J.; Hansen, H. C. B.; Plackett, D. *J. Appl. Polym. Sci.* **2011**,
665   *122*, 112.

666   32. Rhim, J. W.; Hong, S. I.; Ha, C. S. *LWT - Food Sci. Technol.* **2009**, *42*, 612.

667   33. López-Rodríguez, N.; Martínez De Arenaza, I.; Meaurio, E.; Sarasua, J. R. *RSC Adv.* **2015**, *5*, 34525.

668   34. Righetti, M. C.; Gazzano, M.; Di Lorenzo, M. L.; Androsch, R. Enthalpy of melting of α′- and α-crystals
669   of poly(L-lactic acid). *Eur. Polym. J.* **2015**, *70*, 215–220.

670   35. Zuza, E.; Ugartemendia, J. M.; Lopez, A.; Meaurio, E.; Lejardi, A.; Sarasua, J. R. *Polymer.* **2008**, *49*,
671   4427.

672   36. Saiter, A.; Delpouve, N.; Dargent, E.; Oberhauser, W.; Conzatti, L.; Cicogna, F.; Passaglia, E. *Eur.*
673   *Polym. J.* **2016**, *78*, 274.

674   37.   Lorenzo, A. T.; Arnal, M. L.; Albuerne, J.; Müller, A. J. *Polym. Test.* **2007**, *26*, 222.

675   38.   Pan, P.; Han, L.; Shan, G.; Bao, Y. *Macromolecules* **2014**, *47*, 8126.

676   39.   Lohmeijer, P. J. A.; Goossens, J. G. P.; Peters, G. W. M. *J. Appl. Polym. Sci.* **2017**, *134*, 2.

677   40.   Krikorian, V.; Pochan, D. J. *Macromolecules* **2004**, *37*, 6480.

678   41.   Li, X.; Yin, J.; Yu, Z.; Yan, S.; Lu, X.; Wang, Y.; Cao, B.; Chen, X. *Polym. Compos.* **2009**, *30*, 1338.

679   42.   Lee, S.-H.; Wang, S.; Teramoto, Y. *J. Appl. Polym. Sci.* **2008**, *108*, 870.

680   43.   Ambrosio-Martín, J.; Lopez-Rubio, A.; Fabra, M. J.; Gorrasi, G.; Pantani, R.; Lagaron, J. M. *J. Appl.*
681   *Polym. Sci.* **2015**, *132*, 1.

682   44.   Pei, A.; Zhou, Q.; Berglund, L. A. *Compos. Sci. Technol.* **2010**, *70*, 815.

683   45.   Arnoult, M.; Dargent, E.; Mano, J. F. *Polymer.* **2007**, *48*, 1012.

684   46.   Henricks, J.; Boyum, M.; Zheng, W. *J. Therm. Anal. Calorim.* **2015**, *120*, 1765.

685   47.   Magoń, A.; Pyda, M. *Polymer.* **2009**, *50*, 3967.

686   48.   Righetti, M. C.; Tombari, E. *Thermochim. Acta* **2011**, *522*, 118.

687   49.   Lin, J.; Shenogin, S.; Nazarenko, S. *Polymer.* **2002**, *43*, 4733.

688   50.   Gao, F. *Mater. Today* **2004**, *7*, 50.

689

690

691

692